



Article

# Dual-Warhead Conjugate Based on Fibroblast Growth Factor 2 Dimer Loaded with $\alpha$ -Amanitin and Monomethyl Auristatin E Exhibits Superior Cytotoxicity towards Cancer Cells Overproducing Fibroblast Growth Factor Receptor 1

Daria Nawrocka , Mateusz Adam Krzyscik <sup>†</sup> , Katarzyna Dominika Sluzalska and Jacek Otlewski <sup>\*</sup>

Department of Protein Engineering, Faculty of Biotechnology, University of Wrocław, Joliot-Curie 14a, 50-383 Wrocław, Poland; daria.nawrocka@uwr.edu.pl (D.N.); mkrzysc1@jhu.edu (M.A.K.); katarzyna.sluzalska@uwr.edu.pl (K.D.S.)

<sup>\*</sup> Correspondence: jacek.otlewski@uwr.edu.pl; Tel.: +48-71-375-28-24

<sup>†</sup> Current address: Institute for NanoBioTechnology, Whiting School of Engineering, Johns Hopkins University, 3400 N Charles St., Baltimore, MD 21218, USA.

**Abstract:** Targeting fibroblast growth factor receptor 1 (FGFR1) is a promising therapeutic strategy for various cancers associated with alterations in the FGFR1 gene. In this study, we developed a highly cytotoxic bioconjugate based on fibroblast growth factor 2 (FGF2), which is a natural ligand of this receptor, and two potent cytotoxic drugs— $\alpha$ -amanitin and monomethyl auristatin E—with completely independent mechanistic modes of action. Utilizing recombinant DNA technology, we produced an FGF2 N- to C-end dimer that exhibited superior internalization capacity in FGFR1-positive cells. The drugs were site-specifically attached to the targeting protein using SnoopLigase and evolved sortase A-mediated ligations. The resulting dimeric dual-warhead conjugate selectively binds to the FGFR1 and utilizes receptor-mediated endocytosis to enter the cells. Moreover, our results demonstrate that the developed conjugate exhibits about 10-fold higher cytotoxic potency against FGFR1-positive cell lines than an equimolar mixture of single-warhead conjugates. The diversified mode of action of the dual-warhead conjugate may help to overcome the potential acquired resistance of FGFR1-overproducing cancer cells to single cytotoxic drugs.

**Keywords:** fibroblast growth factor 2 (FGF2); dimerization; MMAE;  $\alpha$ -amanitin; protein-drug conjugates; sortase A; SnoopLigase; targeted cancer therapy



**Citation:** Nawrocka, D.; Krzyscik, M.A.; Sluzalska, K.D.; Otlewski, J. Dual-Warhead Conjugate Based on Fibroblast Growth Factor 2 Dimer Loaded with  $\alpha$ -Amanitin and Monomethyl Auristatin E Exhibits Superior Cytotoxicity towards Cancer Cells Overproducing Fibroblast Growth Factor Receptor 1. *Int. J. Mol. Sci.* **2023**, *24*, 10143. <https://doi.org/10.3390/ijms241210143>

Academic Editor: Roberto Ronca

Received: 12 May 2023

Revised: 12 June 2023

Accepted: 13 June 2023

Published: 14 June 2023



**Copyright:** © 2023 by the authors. Licensee MDPI, Basel, Switzerland. This article is an open access article distributed under the terms and conditions of the Creative Commons Attribution (CC BY) license (<https://creativecommons.org/licenses/by/4.0/>).

## 1. Introduction

Alterations in the fibroblast growth factor receptor 1 (FGFR1) have been linked to the development and progression of several types of cancer, including breast, lung, gastric, bladder, and ovarian cancers, and is associated with poor prognosis and resistance to chemotherapy [1–3]. FGFR1 signaling is involved in multiple pathways that promote cancer cell proliferation, survival, angiogenesis, and tumor progression, making FGFR1 an attractive therapeutic target in cancer treatment [4,5].

FGFR-targeted therapies have emerged as a promising approach to inhibit FGFR1 signaling and selectively target cancer cells with FGFR1 overexpression. To date, several strategies have been developed, including small molecule inhibitors [6] and monoclonal antibodies [7]. Small molecule FGFR inhibitors are designed to block the ATP binding site of FGFR1, preventing ATP-dependent phosphorylation and downstream signaling. These inhibitors exhibit varying degrees of selectivity against FGFR isoforms and have shown promising results in preclinical and clinical studies. Examples of small-molecule FGFR inhibitors include erdafitinib, pemigatinib, and infigratinib, among others [8–15]. Monoclonal antibodies targeting FGFR1 aim to block FGFR1 activation by inhibiting ligand binding or receptor dimerization. These antibodies can interfere with FGFR1 signaling

and trigger immune-mediated mechanisms of action, such as antibody-dependent cellular cytotoxicity (ADCC) and complement-dependent cytotoxicity (CDC). Clinical trials evaluating FGFR1-targeted monoclonal antibodies, such as bemarituzumab and futibatinib, are underway in various cancer types [16–23].

Several preclinical and clinical studies have shown promising outcomes for treatments targeting FGFR1, demonstrating encouraging response rates and manageable toxicity profiles. However, similar to other targeted therapies, resistance to FGFR1 inhibitors can emerge, either through mutations in the target protein or activation of bypass pathways [24,25]. Thus, to overcome the resistance, it is necessary to utilize combination therapies or sequential treatment with different FGFR1 inhibitors.

Previously, we demonstrated the efficacy of fibroblast growth factor 1 (FGF1) and 2 (FGF2) as a targeting molecules for FGFR1-overproducing cancer cells. These natural FGFR1 ligands, when conjugated with a potent anticancer drug, such as monomethyl auristatin E (MMAE), exhibited a highly selective cytotoxic effect against cancer cells [26–29]. In addition, the cytotoxicity of FGF2-based conjugates was improved by adding two mechanistically distinct warheads [30,31]. Furthermore, we engineered FGF2 dimers that demonstrated remarkable stability and exceptional internalization efficiency into cells overproducing FGFR1 [32]. Achieving efficient internalization of bioconjugates is critical for developing delivery systems for highly cytotoxic drugs. Here, we expand on the FGF-based targeted anti-cancer cytotoxic drug approach by applying the FGF2 dimer as a targeting molecule and through conjugation of two cytotoxic agents with independent modes of action: the antimetabolic agent MMAE and the RNA polymerase II and III inhibitor  $\alpha$ -amanitin ( $\alpha$ AMTN) using two enzymatic ligations. Application of the FGF2 dimer extended by N- and C-terminal peptide tags recognized, respectively, by SnoopLigase and sortase A as a drug delivery vehicle enabled site-specific conjugation of each cytotoxic payload and allowed for precise control over each conjugation step, allowing stoichiometrically defined conjugates to be obtained.

Our results show that the developed conjugate efficiently targets FGFR1-positive cancer cells, leading to excellent and selective toxicity. Compared with single-drug monomeric conjugates, the dimeric FGF2 dual warhead conjugate kills cancer cells more efficiently and has the potential to limit the ability of cancer cells to develop resistance to cytotoxic drugs.

## 2. Results and Discussion

### 2.1. Engineering the Dimeric Dual-Warhead FGF2 Conjugate

#### 2.1.1. Design Principle of the FGF2 Dimer (dFGF2<sub>V1V2</sub>)

Our recent report highlights the successful synthesis of FGF2 dimers with variations in both topology and length of the linker used for dimerization [32]. The engineered dimers remained functional in terms of FGFR downstream signaling activation and demonstrated remarkable stability. One of the major findings from the previous study was that the arrangement of FGF2 molecules within the dimer is a crucial factor in facilitating effective internalization into cells that overproduce FGFR1. Achieving efficient internalization of bioconjugates is critical in the development of delivery systems for highly cytotoxic drugs. This allows for the specific release of the active form of the cytotoxic compound exclusively within the targeted cells [33].

Based on our results, we have identified the N- to C-end FGF2 dimer coupled by a ~90 Å length flexible linker (N-PEG12-C dimer) as the most promising candidate for use as a drug carrier, due to its exceptional efficiency in promoting FGFR1-dependent cellular uptake [32]. For the purpose of the current study, we designed and produced in bacterial expression system a dimer whose structure closely resembled that of a chemical N-PEG12-C dimer. We opted to apply recombinant DNA technology in order to streamline the production process of the dimer as much as possible and to optimize its efficiency. The dimer developed in this study consisted of two FGF2 monomers' variants. The first variant in the sequence had a C-terminal GSKSK linker and C78S C96S point mutations, while the second variant contained an N-terminal KCKSGG linker and C78S C96S point mutations. To

separate discrete FGF2 domains within the dimer, we used a flexible glycine-rich synthetic amino acid linker, (SGG)<sub>11</sub> [34,35]. The number of repeating SGG motifs was determined so that the length of the spacer corresponded to the length of the chemical linker applied in the N-PEG12-C dimer. Additionally, we fused an N-terminal DIPATYEFTDGHYITNEPIPPK and C-terminal LPETGG motifs to enable enzymatic attachment of cytotoxic drugs using SnoopLigase and evolved sortase A (eSrtA). We called the resulting FGF2 dimer dFGF2<sub>V1V2</sub> (Figure 1C).

### 2.1.2. $\alpha$ -AMTN and MMAE Conjugation Reaction Scheme

In the pursuit of developing a potent dimeric FGF2 dual-warhead conjugate, our payloads of choice were  $\alpha$ -amanitin ( $\alpha$ -AMTN) and monomethyl auristatin E (MMAE), two powerful drugs that exert diverse mechanisms of action [36].  $\alpha$ -AMTN is a toxic cyclic peptide derived from *Amanita* mushroom species. Its cytotoxic action stems from its selective binding to RNA polymerase II in eukaryotic cells, thereby inhibiting DNA transcription and leading to cell death. Moreover, due to its hydrophilic structure, it is not effectively removed by multi-drug resistant transporters [37,38]. This feature makes it potentially useful for targeting cancer cells that are resistant to other drugs. MMAE, on the other hand, is a synthetic analog of dolastatin 10, a natural anticancer compound. MMAE works by affecting tubulin polymerization, which is crucial for cell division. This disruption to cell division results in cell death, making MMAE a common payload in many antibody–drug conjugates (ADCs) [39–41]. The combination of  $\alpha$ -amanitin and MMAE in a dual-warhead conjugate is anticipated to provide several advantages, including: (i) diverse mechanisms of action: the conjugate can target cancer cells through multiple pathways, increasing the likelihood of effectively killing them and overcoming resistance mechanisms [36]; (ii) synergistic effects: the combination of the two cytotoxic agents may produce a synergistic effect, where their combined action is greater than the sum of their individual effects, enhancing therapeutic efficacy [42]; (iii) overcoming drug resistance: the simultaneous targeting of cancer cells through different mechanisms can help circumvent drug resistance, as the cancer cells are less likely to develop resistance to both drugs at the same time [43].

Our conjugation strategy was based on direct enzymatic ligation. Enzymatic ligation is often considered a better approach than chemical conjugation in the context of drug to protein conjugation for several reasons. First, it can be highly specific, allowing for the selective modification of a single amino acid residue on a protein [44]. In contrast, chemical conjugation can result in non-specific modification of multiple sites, which can lead to decreased protein activity and/or stability [45]. Second, enzymatic ligation can be more efficient than chemical conjugation, as it can occur under mild conditions and does not require harsh chemicals or elevated temperatures that can damage proteins. This can result in higher yields and better preservation of protein activity [46,47]. Third, enzymatic ligation can be more versatile than chemical conjugation, as it can accommodate a wider range of drug molecules and protein targets [48].

We produced homogenous FGF2<sub>V1</sub>, FGF2<sub>V2</sub>, and dFGF2<sub>V1V2</sub> and attached  $\alpha$ AMTN and/or MMAE cytotoxic agents via SnoopLigase- or eSrtA-mediated ligation, respectively (Figure 1A–C and Figure 2A). Both drugs contained cathepsin B-cleavable Val-Cit dipeptide with para-aminobenzylcarbamate (PABC) selfimmolative spacer, which facilitated the release of free drug in the cell interior (Figure 1D) [49].

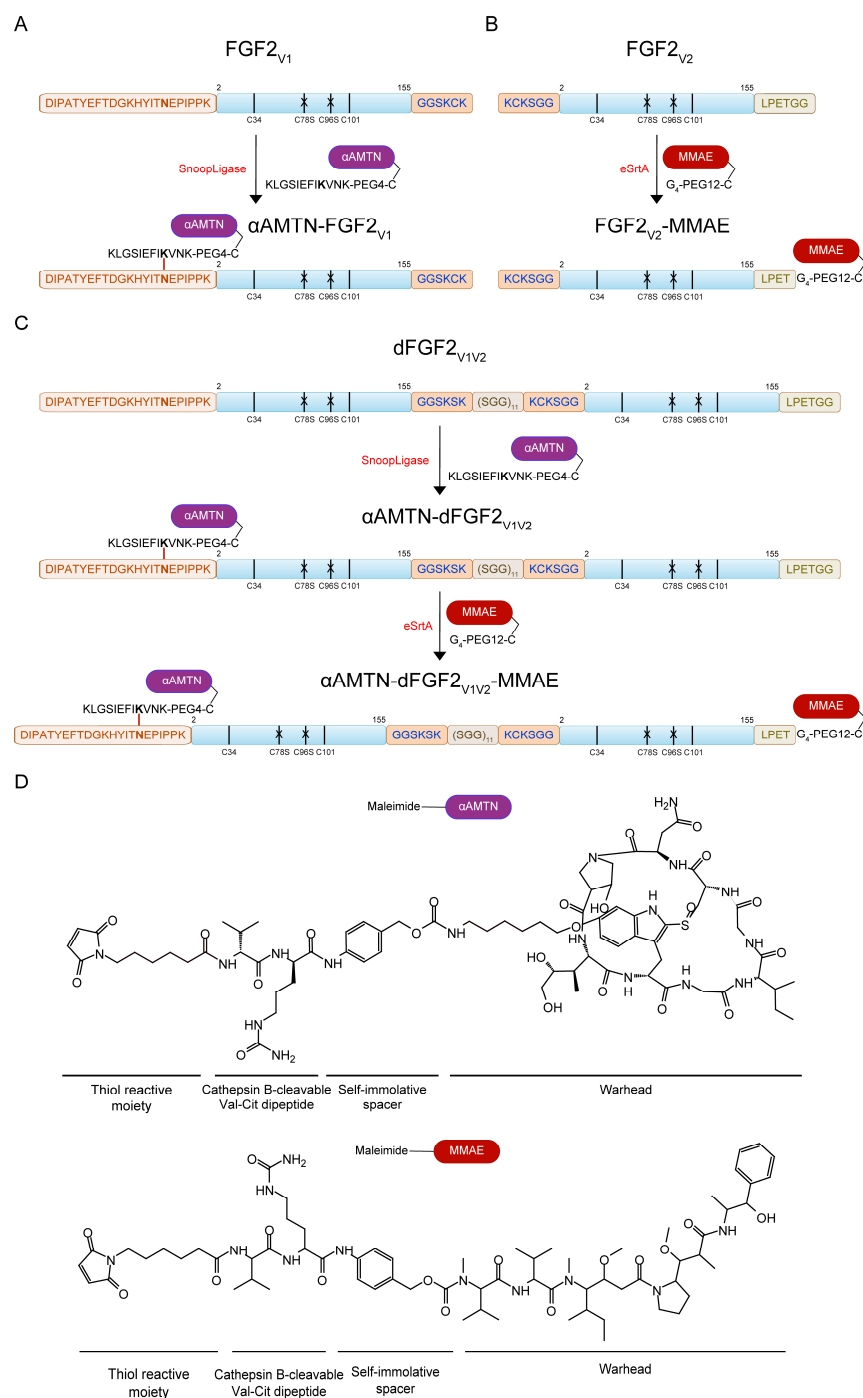


**Figure 1.** Schematic representation of the conjugation procedure. **(A)** Conjugation of  $\alpha$ -amanitin to FGF2<sub>V1</sub> through SnoopLigase-mediated ligation. SnoopLigase promotes an isopeptide bond formation between a reactive asparagine located on the peptide tag attached to the N-terminus of FGF2 and a lysine residue in the sequence of the second peptide that is recognized by the enzyme, coupled with  $\alpha$ -amanitin. **(B)** Conjugation of monomethyl auristatin E to the FGF2<sub>V2</sub> using evolved sortase A. Sortase A recognizes LPETGG motif at the C-terminus of FGF2 and cleaves the threonine-glycine amide bond, then catalyzes the formation of a new peptide bond between the threonine residue and the amino group of a glycine residue on an incoming oligoglycine molecule. **(C)** Schematic of the use of SnoopLigase and sortase A in a two-step procedure of the production of dimeric dual-warhead FGF2 conjugate. **(D)** Structures of maleimide derivatives of  $\alpha$ -amanitin (maleimide- $\alpha$ AMTN) and monomethyl auristatin E (maleimide-MMAE) used for conjugation to FGF2 variants. Both drugs contain a valine–citrulline p-aminobenzylcarbamate linker that is cleaved by intracellular proteases.

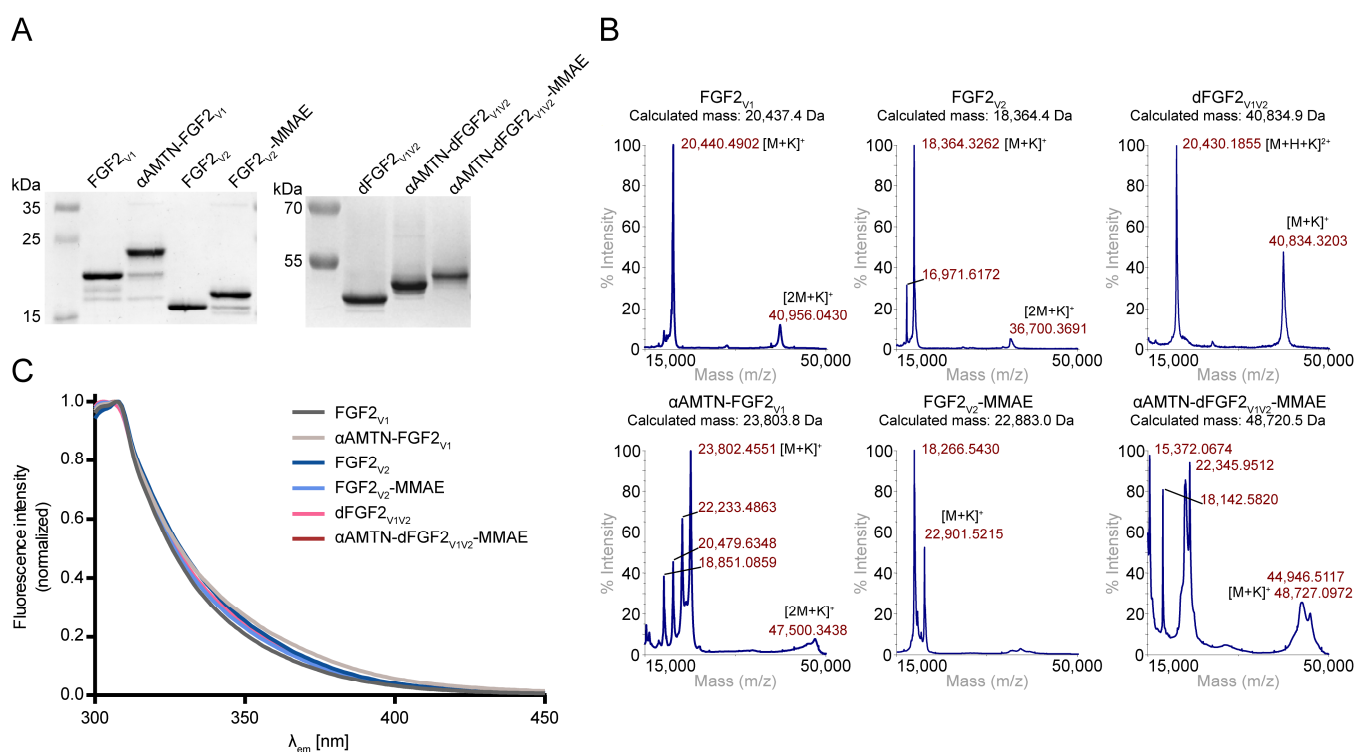


**Figure 2.** Conjugation of FGF2 variants with  $\alpha$ -amanitin and monomethyl auristatin E. **(A)** Electrophoretic analysis of the products of conjugation reactions. **(B)** Mass spectra of FGF2 variants before (upper panel) and after (lower panel) the reaction. **(C)** Fluorescence emission spectra of FGF2 variants and their conjugates. Measurements were performed at a protein concentration of  $4 \times 10^{-6}$  M upon excitation at 280 nm. Curves were normalized to tyrosine emission at 303 nm.

SnoopLigase is a recently discovered enzyme that catalyzes isopeptide bond formation between reactive lysine located on DIPATYEFTDGKHYITNEPIPPK and reactive asparagine on KLGSIIEFIKVNK, in the presence of catalytic glutamic acid located on SnoopLigase. To enable SnoopLigase-mediated covalent conjugation of  $\alpha$ AMTN to FGF2<sub>V1</sub> and dFGF2<sub>V1V2</sub>, first, we synthesized NH<sub>2</sub>-KLGSIIEFIKVNK-Ado<sub>2</sub>-C-CONH<sub>2</sub> peptide (KLGSIIEFIKVNK-PEG4-C). The SnoopLigase-recognized sequence KLGSIIEFIKVNK was attached to cysteine through an Ado-Ado spacer to increase the hydrophilicity and to avoid steric conflicts between FGF2 and peptide-drug conjugate. Then, a maleimide derivative of  $\alpha$ -amanitin (maleimide- $\alpha$ AMTN) (Figure 1D) was attached to KLGSIIEFIKVNK-PEG4-C via a maleimide-thiol reaction. SnoopLigase efficiently ligated KLGSIIEFIKVNK-PEG4-C-vc $\alpha$ AMTN peptide to DIPATYEFTDGKHYITNEPIPPK fusion proteins (FGF2<sub>V1</sub>, dFGF2<sub>V1V2</sub>), resulting in  $\alpha$ AMTN-FGF2<sub>V1</sub> and  $\alpha$ AMTN-dFGF2<sub>V1V2</sub> conjugates. The homogeneity and purity of the products was demonstrated by SDS-PAGE (Figure 2A).

For a site-specific conjugation of MMAE, we employed eSrtA (Figure 1B,C) that was catalytically optimized by a yeast display screening [50]. The eSrtA is a sequence-specific protease with a transpeptidase activity. The enzyme recognizes a LPXTG motif (X is typically any amino acid residue) and cleaves the threonine-glycine amide bond using the cysteine residue as a nucleophile. The resulting acyl-enzyme intermediate is aminolyzed by the attack of an incoming oligoglycine molecule, leading to the formation of a new peptide bond and fusion of the LPXT- and oligoglycine-linked peptides or proteins [51,52]. To conjugate MMAE to the FGF2<sub>V2</sub> and  $\alpha$ AMTN-FGF2<sub>V1</sub> via eSrtA-mediated ligation, we synthesized NH<sub>2</sub>-GGGG-Ado<sub>6</sub>-C-CONH<sub>2</sub> peptide (GGG-PEG12-C) and attached a maleimide derivative of monomethyl auristatin E (maleimide-MMAE) (Figure 1D) via maleimide-thiol chemistry. Next, we added excessive concentrations of GGG-PEG12-C-vcMMAE over FGF2<sub>V2</sub> protein and  $\alpha$ AMTN-dFGF2<sub>V1V2</sub> conjugate to fully convert FGF2<sub>V2</sub>

to FGF2<sub>V2</sub>-MMAE and  $\alpha$ AMTN-dFGF2<sub>V1V2</sub> to  $\alpha$ AMTN-dFGF2<sub>V1V2</sub>-MMAE, as demonstrated by SDS-PAGE (Figure 2A).

We confirmed the identity of FGF2<sub>V1</sub>, FGF2<sub>V2</sub>, dFGF2<sub>V1V2</sub> proteins and their conjugates with  $\alpha$ AMTN and/or MMAE with MALDI-MS (Figure 2B). Additional signals observed in the spectra arose from the fragmentation of the analyte molecules during the desorption/ionization process [53].

Moreover, to assess the proper folding of FGF2<sub>V1</sub>, FGF2<sub>V2</sub>, dFGF2<sub>V1V2</sub> proteins and  $\alpha$ AMTN-FGF2<sub>V1</sub>, FGF2<sub>V2</sub>-MMAE,  $\alpha$ AMTN-dFGF2<sub>V1V2</sub>-MMAE conjugates, we utilized tryptophan fluorescence measurements. In native FGF2, tryptophan fluorescence is quenched by neighboring histidine and proline residues with tyrosine residues dominating the emission spectrum at a maximum of 303 nm. Upon unfolding, the quenching effect is diminished, resulting in a substantial increase in fluorescence at 353 nm. The fluorescence emission spectra indicate the folded native state of all investigated proteins and conjugates (Figure 2C).

## 2.2. Evaluation of FGFR1 Expression Levels and Accessibility for FGF2 in Various Cancer Cell Lines

To determine the cytotoxic potency and FGFR1 selectivity of the dimeric dual-warhead conjugate, we employed a panel of five cancer cell lines with varying FGFR1 levels. We utilized FGFR1-positive NCI-H520 and NCI-H1581 lung carcinomas, JIMT-1 breast ductal carcinoma, and G292 osteosarcoma. We also used HCC95, previously characterized as lung cancer cells with a low physiological FGFR1 levels [54–56]. The expression level of FGFR1 in all tested cell lines was analyzed with Western blotting (Figure 3A). Furthermore, the level of FGFRs accessible for FGF2 was indirectly assessed via flow cytometric measurements of the intensity of the fluorescent signal coming from DyLight 650-labeled FGF2 internalized to the cells or bound to the cell surface (Figure 3B–F and Table S1). The strongest signal from the fluorophore-tagged FGF2 was detected in NCI-H520 cells (Figure 3C), consistent with the high expression level of FGFR1 in these cells. NCI-H1581 (Figure 3D), JIMT-1 (Figure 3E) and G292 (Figure 3F) cells also accumulated significant or intermediate levels of FGF2. A detectable signal from the fluorescently labeled FGF2 was observed in HCC95 cells as well (Figure 3B), although it was significantly lower than in the other cell lines (Table S1). This finding aligns with previous reports indicating HCC95 is a cell line with low levels, but not devoid, of FGFR1 [54,57]. The data clearly suggest that FGF2 internalization primarily occurs through receptor-mediated endocytosis. Moreover, the different cell lines displayed distinct FGF2 internalization efficiencies, likely due to variations in FGFR1 levels on their surfaces.

## 2.3. Superior Cytotoxicity of the Dimeric Dual-Warhead Conjugate

The main aim of this study was evaluation of the cytotoxic potency of  $\alpha$ AMTN-dFGF2<sub>V1V2</sub>-MMAE conjugate against cancer cell lines exhibiting overexpression of FGFR1. For this purpose, each cell line utilized in the experiment was treated with increasing concentrations of  $\alpha$ AMTN-dFGF2<sub>V1V2</sub>-MMAE, nondimerized  $\alpha$ AMTN-FGF2<sub>V1</sub> and FGF2<sub>V2</sub>-MMAE conjugates mixed in equimolar ratio ( $\alpha$ AMTN-FGF2<sub>V1</sub> + FGF2<sub>V2</sub>-MMAE),  $\alpha$ AMTN-FGF2<sub>V1</sub>, FGF2<sub>V2</sub>-MMAE,  $\alpha$ AMTN, and MMAE. Cytotoxicity was assessed after 96 h of continuous exposure. The EC<sub>50</sub> values were calculated from the Hill equation and are presented in Table 1.

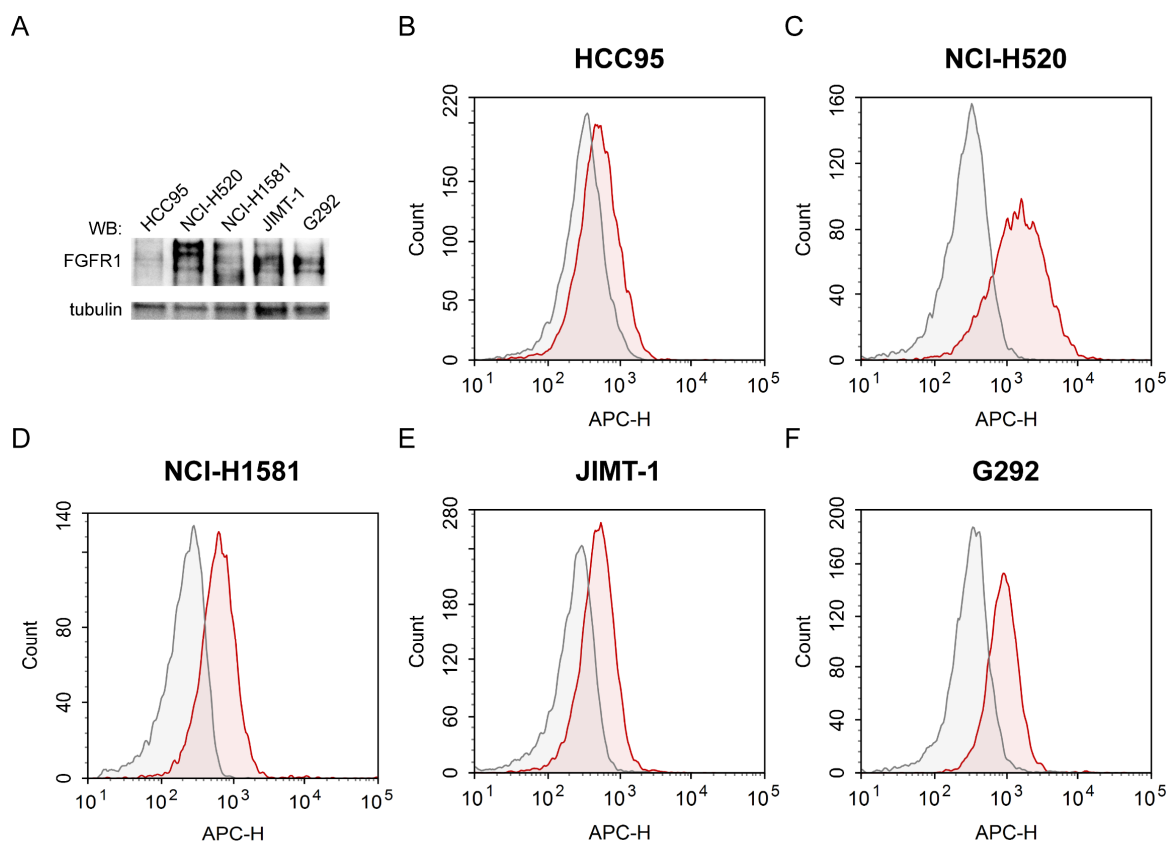


**Figure 3.** Determination of the FGFR1 level and its accessibility to FGF2. (A) Protein levels of FGFR1 in all cancer cell lines incorporated for the study, determined via Western blotting. The level of tubulin served as a loading control. (B–F) Flow cytometric analysis of FGF2 binding and cellular internalization. The cells were incubated on ice with 20 nM DyLight 650-labeled FGF2 for 40 min, then transferred to 37 °C for 30 min. Representative results of three independent experiments are shown.

**Table 1.** Comparison of the cytotoxic effects of conjugates and free drugs on different cell lines with varying levels of FGFR1.

| Preparation   | Cell Line                   |                   |              |              |              |
|---|-----------------------------|-------------------|--------------|--------------|--------------|
|   | HCC95                       | NCI-H520          | NCI-H1581    | JIMT-1       | G292         |
|   | <b>EC<sub>50</sub> [nM]</b> |                   |              |              |              |
| Non-conjugated αAMTN                                | 1238 **                     | n.t. <sup>a</sup> | 998.6 **     | 1278 **      | 967.1 **     |
| Non-conjugated MMAE                                 | 0.3398 **                   | 0.2761 **         | 0.2288 **    | 0.09179 *    | 0.09103 **   |
| αAMTN-FGF2 <sub>V1</sub>                            | 487.7 ***                   | 205.5 ***         | 233.2 **     | 112.5 **     | 225.6 **     |
| FGF2 <sub>V2</sub> -MMAE                            | 91.53 **                    | 82.67 ***         | 22.60 **     | 12.83 *      | 10.77 *      |
| αAMTN-FGF2 <sub>V1</sub> + FGF2 <sub>V2</sub> -MMAE | 52.29                       | 73.46 ***         | 23.28 ***    | 16.40 **     | 14.45 **     |
| <b>αAMTN-FGF2<sub>V1V2</sub>-MMAE</b>               | <b>32.45</b>                | <b>6.803</b>      | <b>2.195</b> | <b>1.304</b> | <b>2.510</b> |

<sup>a</sup> n.t., Nontoxic in the studied concentration range; *t* test of three independent experiments was performed for statistical analysis of data. Statistical significance (versus αAMTN-FGF2<sub>V1V2</sub>-MMAE group): \* *p* < 0.05, \*\* *p* < 0.01, \*\*\* *p* < 0.001. Bold indicate the molecule that was developed and described.

As shown in Figure 4, αAMTN-dFGF2<sub>V1V2</sub>-MMAE exhibited superior cytotoxicity against all investigated FGFR1-overexpressing cells, surpassing both monosubstituted αAMTN-FGF2<sub>V1</sub> and FGF2<sub>V2</sub>-MMAE conjugates used in monotherapy, as well as combination therapy with equimolarly mixed αAMTN-FGF2<sub>V1</sub> and FGF2<sub>V2</sub>-MMAE. In the case of HCC95, partial cytotoxicity was observed with FGF2<sub>V2</sub>-MMAE and αAMTN-dFGF2<sub>V1V2</sub>-MMAE at the highest tested concentration (Figure 4A). This phenomenon could potentially be attributed to the presence of low physiological levels of FGFR1 on the surface of HCC95

cells. Alternatively, there might be some target-independent toxicity of MMAE released from the conjugates. All tested conjugates exhibited cytotoxicity against FGFR1-positive cell lines: NCI-H520, NCI-H1581, JIMT-1 and G292 in a concentration-dependent manner. Interestingly, NCI-H520 cell line characterized by relatively high FGFR1 level (Figure 3A) and the most efficient cellular uptake of wild-type FGF2 (Figure 3B), was barely sensitive to single FGF2 conjugates with  $\alpha$ AMTN or MMAE (including the mixture of both) in a studied concentration range (Figure 4B). However, application of the  $\alpha$ AMTN-dFGF2<sub>V1V2</sub>-MMAE dimeric dual-warhead conjugate led to a significant reduction in cell viability, with a decrease of over 90% observed at the highest tested concentration (Figure 4B). The calculated EC<sub>50</sub> value of the dimeric conjugate was more than 10 times lower compared to equimolarly mixed  $\alpha$ AMTN-FGF2<sub>V1</sub> and FGF2<sub>V2</sub>-MMAE. Similar outcomes were observed in other cell lines with high FGFR1 expression levels. The EC<sub>50</sub> values of  $\alpha$ AMTN-dFGF2<sub>V1V2</sub>-MMAE were in the low nanomolar range and were at least one order of magnitude lower compared to the EC<sub>50</sub> of mixed  $\alpha$ AMTN-FGF2<sub>V1</sub> and FGF2<sub>V2</sub>-MMAE, except for G292 cells, where, nonetheless, a large 5.8-fold reduction in EC<sub>50</sub> was evident (Table 1, Figure 4C–E).

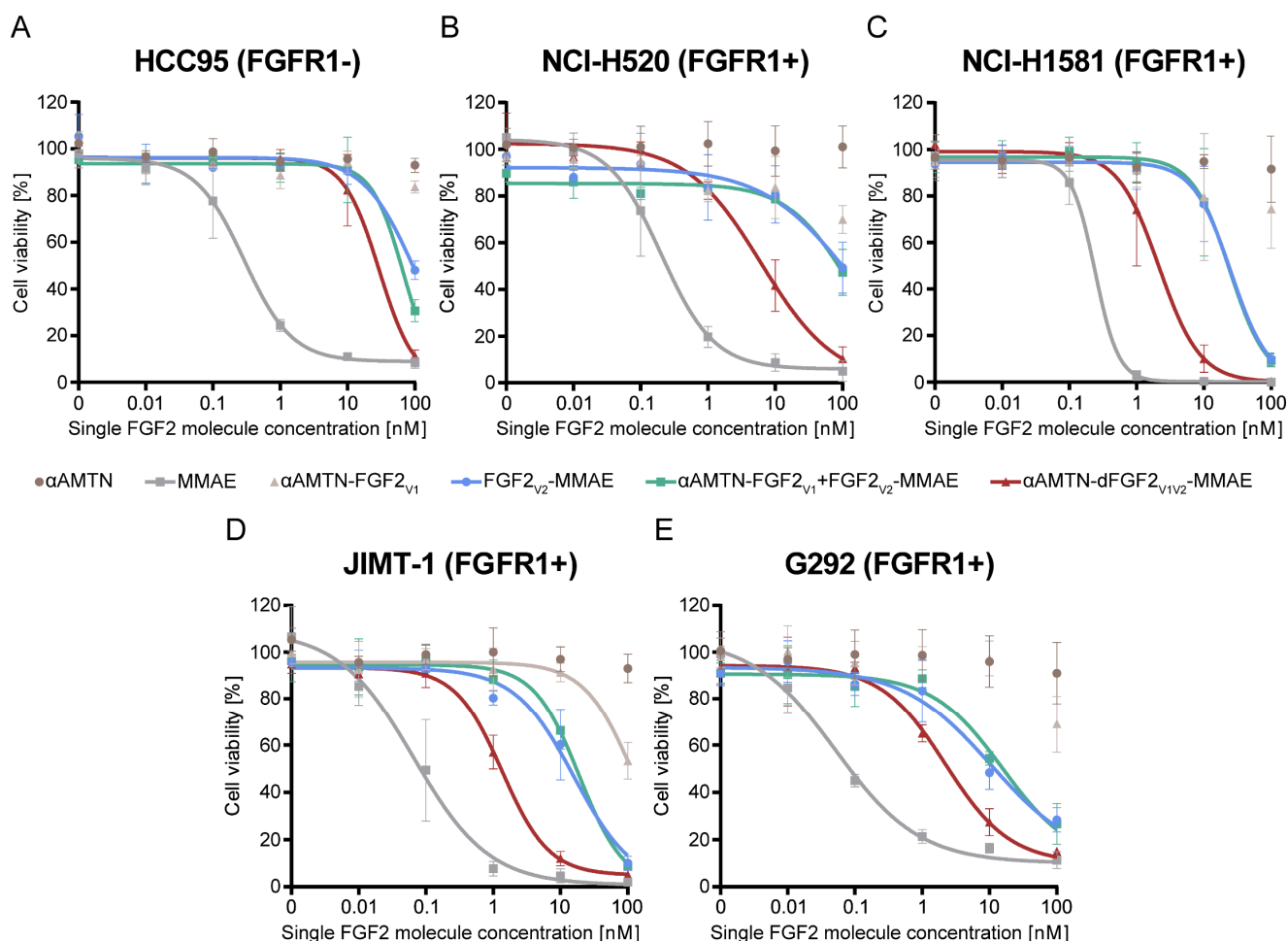


**Figure 4.** Cytotoxicity of the dimeric dual-warhead FGF2 conjugate against HCC95 control cell line with low physiological FGFR1 level (A) and FGFR1-overproducing cells (B–E). Viability of cells treated with the increasing concentrations of the  $\alpha$ AMTN-dFGF2<sub>V1V2</sub>-MMAE,  $\alpha$ AMTN-FGF2<sub>V1</sub> and FGF2<sub>V2</sub>-MMAE conjugates applied individually or in combination therapy, as well as free drugs. The concentrations of all conjugates were normalized to the molar concentration of FGF2 molecules in the preparation. The presented data are mean values from three experiments  $\pm$  SD. The solid lines represent Hill equation fits.

The EC<sub>50</sub> values of  $\alpha$ AMTN-dFGF2<sub>V1V2</sub>-MMAE and mixed single-drug FGF2 conjugates, calculated for the FGFR1-low HCC95 cell line, were comparable and significantly higher than the EC<sub>50</sub> values calculated for other FGFR1-positive cell lines. A very low response observed in the FGFR1-deficient cell line indicates that the dimeric FGF2 dual-warhead conjugate exhibits excellent selectivity towards FGFR1-expressing cells.

In all studied cell lines, it has been observed that the conjugate of  $\alpha$ AMTN was more toxic than free non-conjugated  $\alpha$ AMTN, but the conjugate of MMAE was less toxic than free non-conjugated MMAE. The hydrophilic nature of  $\alpha$ AMTN limits its efficient uptake by cancer cells, thereby reducing its ability to exert cytotoxic effects on the target cells [58,59]. In contrast, free MMAE is able to freely pass through cellular membranes, which allows it to exert its cytotoxic activity without limitations in cellular delivery, though it may lack selectivity [60,61]. However, when  $\alpha$ AMTN and MMAE are conjugated to the FGF2 targeting protein, the conjugates utilize FGFR1-mediated endocytosis for cellular delivery, ensuring selectivity towards FGFR1-bearing cells. These findings highlight the efficiency of FGF2 as a targeting molecule in the conjugates.

#### 2.4. Selective and Efficient Internalization of the $\alpha$ AMTN-dFGF2<sub>V1V2</sub>-MMAE Conjugate into Cells Expressing FGFR1

The success of cytotoxic conjugate-based anticancer therapy largely depends on the targeted delivery of toxic drugs, specifically to cancer cells. As we observed that the internalization capacity of wild-type FGF2 did not entirely correlate with the sensitivity of cell lines towards FGF2 conjugates, we further examined the internalization of all investigated conjugates using the same panel of cell lines that were used for cytotoxicity evaluation. To assess internalization efficiency, we labeled the FGF2 conjugates with a fluorescent probe and quantified their uptake using flow cytometry at a concentration close to the EC<sub>50</sub> value of the dimeric conjugate (2 nM) (Figure 5). We aimed to determine if the shift in cytotoxicity towards lower concentrations was due to a higher internalization yield of the dimeric conjugate at low concentrations. To eliminate non-internalized fluorophore-labeled preparations from the cell surface, we incorporated acid washing as a step in our experimental protocol. Analysis of the internalization yield revealed that the  $\alpha$ AMTN-dFGF2<sub>V1V2</sub>-MMAE dimeric conjugate exhibited significantly enhanced cell uptake efficiency compared to both the  $\alpha$ AMTN-FGF2<sub>V1</sub> and FGF2<sub>V2</sub>-MMAE monosubstituted conjugates, as well as the mixture of both, in the case of all FGFR1-overexpressing cell lines, but not in FGFR1-low HCC95 cells. The relative fluorescence intensity increase in HCC95 cells treated with  $\alpha$ AMTN-dFGF2<sub>V1V2</sub>-MMAE was more than twice as low as that observed for cells treated with the combination of  $\alpha$ AMTN-FGF2<sub>V1</sub> + FGF2<sub>V2</sub>-MMAE. These data confirm that  $\alpha$ AMTN-dFGF2<sub>V1V2</sub>-MMAE is an effective and selective conjugate for targeting FGFR1-positive cancer cells. Furthermore, the strong cytotoxicity displayed at low nanomolar concentrations aligns well with the internalization efficiency, substantiating the FGF2-mediated selective delivery mechanism responsible for the observed cytotoxic effects.

$\alpha$ AMTN-dFGF2<sub>V1V2</sub>-MMAE had a greater cytotoxic effect than any of the single-drug FGF2 conjugates, which could be explained as a result of the combined cytotoxic action of  $\alpha$ AMTN and MMAE. Previously, we synthesized a bifunctional FGF2 conjugate, incorporating both  $\alpha$ AMTN and MMAE as cytotoxic agents. These moieties were covalently linked to a cysteine residue through maleimide chemistry and propargyl lysine utilizing copper(I)-catalyzed azide-alkyne 1,3-dipolar cycloaddition (CuAAC), respectively. This dual-warhead conjugate exhibited enhanced cytotoxic efficacy against cancer cell lines with FGFR1 overexpression, surpassing the performance of single-drug conjugates [30]. We also produced a modular dual-warhead conjugate comprising two monosubstituted FGF2 molecules joined together via eSrtA-mediated ligation and demonstrated that conjugate containing both  $\alpha$ AMTN and MMAE shows a greater cytotoxic effect than any of the single-drug FGF2 conjugates [31]. However, the dimerization method utilized previously requires a two-step enzymatic reaction compared to the bacterial production of the N-to-C dFGF2<sub>V1V2</sub> dimer described here. Additionally, the previously utilized C-to-C dimer

shows lower internalization efficacy compared to the N-to-C-end dFGF2<sub>V1V2</sub> dimer. In our current study, we demonstrate that the utilization of a dimeric dual-warhead conjugate could be a highly promising approach, enhancing the efficacy of cancer therapies while minimizing potential side effects. This is attributed to the superior internalization capacity of the dimeric conjugate in cells with high FGFR1 levels, which leads to increased and selective cytotoxicity. Our findings suggest that the use of a dimeric conjugate may offer a more effective and targeted treatment strategy for cancers with high FGFR1 expression, highlighting its potential for improved therapeutic outcomes.

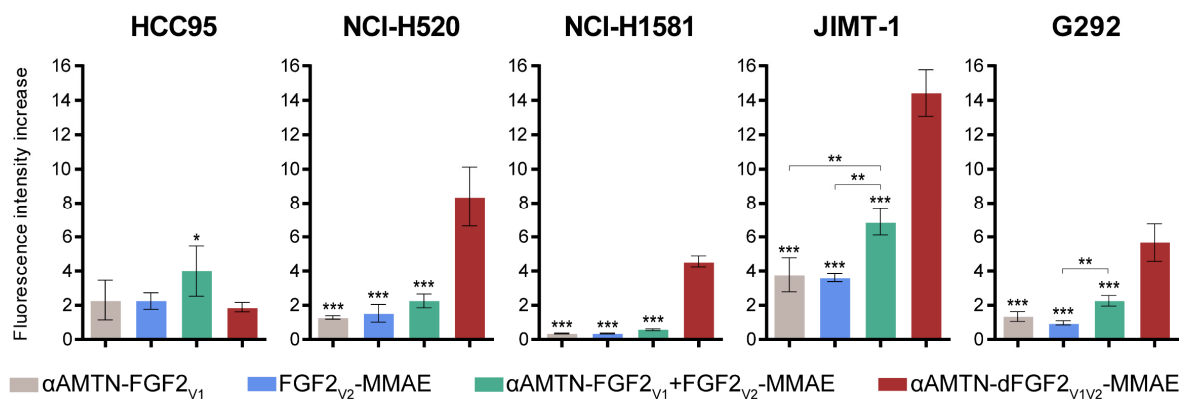


**Figure 5.** Internalization of the  $\alpha$ AMTN-dFGF2<sub>V1V2</sub>-MMAE and  $\alpha$ AMTN-FGF2<sub>V1</sub> and FGF2<sub>V2</sub>-MMAE conjugates used separately or simultaneously in an equimolar ratio. For determination of internalization efficiency, different cancer cell lines were incubated for 15 min at 37 °C with Alexa Fluor 555-labeled conjugates at a concentration of 2 nM (concentrations were normalized to the molar concentration of FGF2 molecules in the preparation). Results represent the relative fluorescence intensities ( $\Delta I/I_0$ ) from three independent experiments. Values of the relative fluorescence intensities are the means for each data set  $\pm$  SD. Statistical significance (versus  $\alpha$ AMTN-dFGF2<sub>V1V2</sub>-MMAE group): \*  $p < 0.05$ , \*\*  $p < 0.01$ , \*\*\*  $p < 0.001$ .

### 3. Materials and Methods

#### 3.1. Reagents

All chemical reagents were procured from commercial sources and utilized as received, without additional purification. Reagents used for the solid-phase peptide synthesis are as follows. Fmoc-Cys(Trt) TentaGels RAM resin (particle size: 90  $\mu$ m, loading 0.2–0.25 mmol/g) purchased from Rapp Polymere GmbH (Tübingen, Germany). Amino acids: Fmoc-L-Lys(Boc)-OH, Fmoc-L-Asn(Trt)-OH, Fmoc-L-Val-OH, Fmoc-L-Ile-OH, Fmoc-L-Phe-OH, Fmoc-L-Glu(OtBu)-OH, Fmoc-L-Ser(tBu)-OH, Fmoc-Gly-OH, Fmoc-L-Leu-OH, Fmoc-O<sub>2</sub>Oc-O<sub>2</sub>Oc-OH piperidine, TIS (triisopropylsilane), DIPEA (*N,N*-diisopropylethylamine), DMF (*N,N'*-dimethylformamide), DCM (dichloromethane), and TFA (trifluoroacetic acid) from Iris Biotech GmbH (Marktredwitz, Germany). HPLC pure acetonitrile and Et<sub>2</sub>O (diethyl ether) were acquired from Avantor (Gliwice, Poland); FA (formic acid), TCA (trichloroacetic acid), and TFA (trifluoroacetic acid) from Merck (Darmstadt, Germany). TCE (2,2,2-trichloroethan-1-ol) was from Santa Cruz Biotechnology (Dallas, TX, USA). DTNB (Ellman's Reagent) (5,5-dithio-bis-(2-nitrobenzoic acid)) was from Thermo Fisher Scientific (Waltham, MA, USA). The toxins:  $\alpha$ -amanitin and MC-vc-PAB-C<sub>6</sub>- $\alpha$ -amanitin were from Levena Biopharma Co., Ltd. (San Diego, CA, USA). MMAE (monomethyl auristatin E) and MC-vc-PAB-MMAE were from MedChemExpress (Monmouth Junction, NJ, USA). Alexa Fluor 555 C<sub>2</sub> Maleimide and DyLight 650 NHS Ester dyes, and alamarBlue reagent were from Thermo Fisher Scientific. The chromatographic columns: HiTrap Desalting with Sephadex G-25 resin, HiTrap Heparin HP and HisTrap HP with Ni-Sepharose media were from GE Healthcare (Chicago, IL, USA). Zeba Spin Desalting columns were from Thermo Fisher Scientific. Synergi 4  $\mu$ m Fusion-RP 80 Å 250  $\times$  10 mm<sup>2</sup> LC column was

from Phenomenex Inc. (Torrance, CA, USA). All other reagents were purchased from Sigma-Aldrich (Saint Louis, MO, USA) or BioShop Canada Inc. (Burlington, ON, USA).

### 3.2. Cell Lines

The NCI-H520 (human squamous cell carcinoma, HTB-182), NCI-H1581 (human non-small cell lung cancer, CRL-5878), and G292 clone A141B1 (human osteosarcoma, CRL-1423) cell lines were obtained from American Type Culture Collection (ATCC, Manassas, VA, USA); JIMT-1 (human breast ductal carcinoma) cells were acquired from the Leibniz Institute DSMZ-German Collection of Microorganisms and Cell Cultures (Braunschweig, Germany); whereas HCC95 cell lines derived from human lung squamous carcinoma were procured from Sigma-Aldrich. NCI-H520 cells were cultured in RPMI 1640 medium from ATCC; NCI-H1581 in RPMI 1640 from BioWest (Nuaillé, France); G292 and JIMT-1 in DMEM High Glucose medium with stable glutamine and sodium pyruvate (BioWest); and HCC95 in RPMI 1640 (ATCC) with the addition of 0.1% sodium bicarbonate (Gibco, Billings, MT, USA). All culture media were supplemented with 10% fetal bovine serum from Thermo Fisher Scientific, and 1% penicillin/streptomycin mix from BioWest. All cell lines were maintained in a humidified incubator at 37 °C in 5% CO<sub>2</sub> atmosphere and were seeded onto tissue culture plates the day before initiating the experiments.

The cell lines used in the study were examined for the presence of the FGFR1 via Western blotting. The cells were lysed in 4× SDS-PAGE loading buffer (200 mM Tris-HCl pH 6.8, 8% SDS, 0.4% bromophenol blue, 50 mM TCEP, 40% glycerol), sonicated, and boiled. Cell lysates were resolved by 10% SDS-PAGE, transferred to the Immobilon-PSQ PVDF 0.2 µm membrane (Millipore, Darmstadt, Germany) and immunoblotted with the primary antibody directed against FGFR1 (#9740) purchased from Cell Signaling (Danvers, MA, USA). Tubulin served as a loading control and was detected with the antibody (#T6557) from Sigma-Aldrich. HRP-conjugated anti-mouse (115-035-003) and anti-rabbit (111-035-144) secondary antibodies were obtained from Jackson Immuno-Research Laboratories (Cambridge, UK).

### 3.3. Recombinant Proteins

For the purpose of this work, three FGF2 variants were used: (a) FGF2 with N-terminal DIPATYEFTDGKHYITNEPIPPK, C-terminal GSKCK motifs and two point mutations (C78S, C96S) (FGF2<sub>V1</sub>), (b) FGF2 with N-terminal KCKSGG, C-terminal LPETGG motifs and two point mutations (C78S, C96S) (FGF2<sub>V2</sub>), and (c) dimer consisting of FGF2<sub>V1</sub> and FGF2<sub>V2</sub> moieties joined by (SGG)<sub>11</sub> linker (dFGF2<sub>V1V2</sub>). The pET-3a and pET-11d plasmids carrying cDNA of FGF2<sub>V1</sub> and dFGF2<sub>V1V2</sub>, respectively, were purchased from the Gene Universal (Newark, DE, USA) as a custom gene synthesis. The LPETGG sequence was introduced to the FGF2 with N-terminal KCKSGG linker and C78S C96S point mutations via site-directed mutagenesis [31]. All FGF2 proteins were produced in *Escherichia coli* (*E. coli*) Rosetta 2(DE3)pLysS (Novagen-EMD Biosciences, Madison, WI, USA). Individual colonies of transformed *E. coli* were grown in LB medium with 100 µg/mL ampicillin and 30 µg/mL chloramphenicol for 16 h at 37 °C, 200 rpm. Overnight cultures were then diluted 1:50 in a TB medium with 100 µg/mL ampicillin and cultivated at 37 °C, 200 rpm to OD<sub>600</sub> 2.0. The protein expression was induced by the addition of IPTG to a final concentration of 0.5 mM. The production of FGF2<sub>V1</sub> was continued for 1h under the same conditions. In turn, cultures of FGF2<sub>V2</sub> and dFGF2<sub>V1V2</sub> were incubated for 16 h at 25 °C (FGF2<sub>V2</sub>) or 16 °C (dFGF2<sub>V1V2</sub>), 200 rpm. The bacteria were harvested via centrifugation at 7500× g, resuspended in 50 mM monosodium phosphate pH 7.4, 0.15 M NaCl, 2 mM DTT, 1 mM EDTA, 0.1% Triton X-100, 1 mM PMSF, 250U Universal Nuclease (Thermo Fisher Scientific), and homogenized via sonication on ice. The cell lysates were centrifuged at 50,000× g at 4 °C for 1 h. The clarified supernatants were diluted with elution buffer (50 mM monosodium phosphate pH 7.4 with 2 M NaCl, 2 mM DTT, 1 mM EDTA, 1 mM NH<sub>4</sub>SO<sub>4</sub>) to a final NaCl concentration of 0.5 M. FGF2 proteins were purified via affinity chromatography using a HiTrap Heparin HP column and NGC chromatography system

(Bio-Rad, Hercules, CA, USA). Proteins were eluted from the column with a linear 0.5–2 M gradient of NaCl, except for dFGF2<sub>V1V2</sub>, where 0.5–3 M gradient was applied.

The pET28a-AviTag-SnoopLigase was a gift from Mark Howarth (Addgene plasmid #105626) [46]. The expression plasmid was transformed into *E. coli* Rosetta 2(DE3)pLysS (Novagen-EMD Biosciences). A single colony of transformed *E. coli* was inoculated into LB medium with 50 µg/mL kanamycin and 30 µg/mL chloramphenicol and incubated for 16 h at 37 °C, 200 rpm. Starter cultures were then diluted 1:50 in TB medium with 50 µg/mL kanamycin and grown at 37 °C, 200 rpm until OD<sub>600</sub> 2.0. Protein expression was induced with 0.42 mM IPTG and protein production was carried out overnight at 30 °C, 200 rpm. SnoopLigase was purified using HisTrap HP column with Ni-Sepharose media. Chromatography was performed on the NGC system (Bio-Rad). The procedure was performed according to the standard protocol for purification of histidine-tagged proteins (GE Healthcare). SnoopLigase was eluted with a linear 10–500 mM gradient of imidazole. Following the elution, protein fraction was desalted using a HiTrap Desalting column with Sephadex G-25 resin. SnoopLigase was stored in TB pH 7.6 (50 mM Tris base adjusted to pH 7.6 with boric acid) with 5% glycerol.

The evolved sortase A pentamutant (eSrtA) in pET29 was a gift from David Liu (Addgene plasmid #75144) [50] and was produced and purified as already described [31].

#### 3.4. Synthesis and Purification of KLSIEFIKVNK-PEG4-C-vcαAMTN and GGGG-PEG12-C-vcMMAE

Synthesis of NH<sub>2</sub>-KLSIEFIKVNK-Ado<sub>2</sub>-C-CONH<sub>2</sub> and NH<sub>2</sub>-GGGG-Ado<sub>6</sub>-C-CONH<sub>2</sub> was performed on solid support according to the solid phase peptide synthesis (SPPS) method described as part of the Fmoc strategy. The peptides were cleaved from the resin with a mixture of TFA/DMC/TIS/H<sub>2</sub>O (vol%, 95:3:1:1) or TFA/DMC/EDT/TIS/H<sub>2</sub>O (vol%, 93:3:2:1:1), respectively. The crude peptides were triply precipitated in cold Et<sub>2</sub>O, purified by reversed-phase high-performance liquid chromatography (RP-HPLC), and lyophilized. Both samples were dissolved in *N,N*-dimethylacetamide (DMAc) and peptides' concentration was estimated by assaying sulfhydryl groups with Ellman's reagent (Thermo Fisher Scientific).

Conjugation of NH<sub>2</sub>-KLSIEFIKVNK-Ado<sub>2</sub>-C-CONH<sub>2</sub> (1.5 µmol) with MC-vc-PAB-C6-α-amanitin (1.0 µmol) was performed in DMAc (275 µL) in the presence of DIPEA (10 µmol). The reaction was carried out for 1 h at room temperature on the rotator with gentle shaking. MC-vc-PAB-MMAE (5 µmol) was conjugated to NH<sub>2</sub>-GGGG-Ado<sub>6</sub>-C-CONH<sub>2</sub> (10 µmol) in 500 µL DMAc with the addition of DIPEA (50 µmol). The reaction was conducted at room temperature for 6 h. The peptide–drug conjugates were purified from the reaction mixtures using RP-HPLC and lyophilized. The identity of the products was confirmed by MALDI-MS.

#### 3.5. Synthesis of the Conjugates

##### 3.5.1. Conjugation of the FGF2<sub>V1</sub> and dFGF2<sub>V1V2</sub> with αAMTN via SnoopLigase-Mediated Ligation

FGF2<sub>V1</sub> and dFGF2<sub>V1V2</sub> proteins containing N-terminal DIPATYEFTDGKHYITNEPIPPK motif were monosubstituted with KLSIEFIKVNK-PEG4-C-vcαAMTN peptide–drug conjugate in the reaction catalyzed by SnoopLigase. FGF2<sub>V1</sub> and dFGF2<sub>V1V2</sub> were transferred into the reaction buffer (25 mM HEPES pH 7.6, 15% glycerol, 2 mM TCEP) using HiTrap Desalting column with Sephadex G-25 resin. KLSIEFIKVNK-PEG4-C-vcαAMTN was dissolved in DMAc to prepare 10 mM stock solution. Next, 10 µM FGF2<sub>V1</sub> or dFGF2<sub>V1V2</sub> was incubated with 80 µM KLSIEFIKVNK-PEG4-C-vcαAMTN and 30 µM SnoopLigase for 24 h at 15 °C. The reaction mixture was then loaded onto a HiTrap Heparin HP column. The excess of nonreacted and nonimmobilized peptide and protein was immediately removed by washing the resin with reaction buffer. However, upon reaction, SnoopLigase strongly binds to the reaction product. To disrupt SnoopLigase–reaction product interaction and allow efficient purification of the ligated product, the column was washed with 3 resin volumes of 2 M imidazole pH 7.0, then washed with 5 resin volumes of 25 mM HEPES pH

7.6, 0.154 M NaCl. The resulting  $\alpha$ AMTN-FGF2<sub>V1</sub> or  $\alpha$ AMTN-dFGF2<sub>V1V2</sub> conjugate, free from SnoopLigase, was eluted from the column with 25 mM HEPES pH 7.6, 2.5 M NaCl, 10 mM Na<sub>2</sub>SO<sub>4</sub>, 5 mM CaCl<sub>2</sub>.

### 3.5.2. Double-Warhead Conjugate Synthesis. Conjugation of the $\alpha$ AMTN-dFGF2<sub>V1V2</sub> and FGF2<sub>V2</sub> with MMAE via eSrtA-Mediated Ligation

GGGG-PEG12-C-vcMMAE peptide–drug conjugate was coupled with  $\alpha$ AMTN-dFGF2<sub>V1V2</sub> conjugate and FGF2<sub>V2</sub> protein containing C-terminal LPETGG sequence using eSrtA. For the reaction,  $\alpha$ AMTN-dFGF2<sub>V1V2</sub> and FGF2<sub>V2</sub> were buffered to 25 mM HEPES pH 7.6, 154 mM NaCl, 10 mM Na<sub>2</sub>SO<sub>4</sub>, 5 mM CaCl<sub>2</sub>, and 2 mM TCEP using a HiTrap Desalting column with Sephadex G-25 resin. The reaction of 40  $\mu$ M  $\alpha$ AMTN-dFGF2<sub>V1V2</sub> or FGF2<sub>V2</sub> with 100  $\mu$ M GGGG-PEG12-C-vcMMAE was carried out in the presence of 0.25  $\mu$ M eSrtA for 4 h at 15 °C. To remove the catalyst and excess reactant, the reaction mixture was passed through a HiTrap Heparin HP column. Unbound molecules were washed off the column with 25 mM HEPES pH 7.6 and the target product of the reaction ( $\alpha$ AMTN-dFGF2<sub>V1V2</sub>-MMAE or FGF2<sub>V2</sub>-MMAE) was eluted with 25 mM HEPES pH 7.6, 2.5 M NaCl, 2 mM TCEP. The efficiency of the conjugation was confirmed by SDS-PAGE. The identity of the conjugates was confirmed by MALDI-MS.

### 3.6. Mass Spectrometry

Molecular masses of peptides, proteins and their conjugates were verified by MALDI-TOF/TOF MS (Applied Biosystems AB 4800+, Waltham, MA, USA).  $\alpha$ -cyano-4-hydroxycinnamic acid or sinapic acid were used as a matrix.

### 3.7. Spectrofluorimetry

Spectrofluorimetric analysis was carried out to determine the folding state of the FGF2 variants and their conjugates. The tryptophan fluorescence spectra were acquired using a FP-750 spectrofluorimeter (Jasco, Tokyo, Japan) with excitation at 280 nm and emission in the 300–450 nm range. Measurements were performed at 20 °C at  $\sim$ 4  $\mu$ M sample concentration in PBS.

### 3.8. Cytotoxicity Assay

The cytotoxicity of the conjugates and free drugs was evaluated on NCI-H520, NCI-H1581, JIMT-1 and G292 cell lines characterized as FGFR1 amplified, as well as on HCC95 with low levels of FGFR1 [54]. Cells were seeded in 96-well plates at a density of  $5 \times 10^5$  cells/well in 100  $\mu$ L of dedicated culture media 24 h prior to commencing the experiment. The media were then replaced with fresh complete media and the cells were treated with six concentrations of conjugate or free drug (0.01 to 100 nM range). The effect of the investigated preparations on cell survival was determined after 96 h of continuous exposure. Cell viability was measured using an alamarBlue reagent, according to the protocol provided by the manufacturer. Fluorescence emission of the reduced form of the reagent at 590 nm, upon excitation at 560 nm, was measured using an Infinite M1000 PRO microplate reader (Tecan, Mannedorf, Switzerland). Cytotoxicity experiments were performed in triplicate. To determine the half maximal effective concentration (EC<sub>50</sub>), the data were fitted to the Hill equation using the GraphPad Prism version 6.01 (GraphPad Software, San Diego, CA, USA). Statistical significance was determined using the paired Student's t-tests assuming equal variance.

### 3.9. Labeling of Conjugates and Wild-Type FGF2 with Fluorescent Probes

Unmodified wild-type FGF2 (FGF2 WT) was labeled with DyLight 650 Succinimidyl Ester; in turn,  $\alpha$ AMTN-FGF2<sub>V1</sub>, FGF2<sub>V2</sub>-MMAE and  $\alpha$ AMTN-dFGF2<sub>V1V2</sub>-MMAE conjugates with Alexa Fluor 555 C<sub>2</sub> Maleimide. For the labeling reaction, proteins were dissolved at 30  $\mu$ M in a suitable buffer—FGF2 WT in 25 mM HEPES pH 8.0, 10 mM Na<sub>2</sub>SO<sub>4</sub>, conjugates in 25 mM HEPES pH 7.4, 10 mM Na<sub>2</sub>SO<sub>4</sub>, and 1 mM TCEP. Fluorescent probes were

reconstituted in DMAc to prepare 10  $\mu$ M stock solutions and were added directly to the proper protein or conjugate solution in a 10-fold molar excess. The reaction was carried out at room temperature for 1 h in the dark. Non-reactive excess fluor reagent was removed from the protein using ZebaSpin Desalting columns (Thermo Fisher Scientific).

### 3.10. Flow Cytometric Evaluation of FGF2 Capacity to Bind to the Cells

The capacity of FGF2 to bind and to enter to the cells differing in total FGFR1 levels was analyzed as we reported earlier, with minor modifications [31]. HCC95, NCI-H520, NCI-H1581, JIMT-1, and G292 cells were seeded at a density of  $5 \times 10^5$  cells/well in a 6-well plate in complete culture medium and left overnight to adhere. The media were then replaced with serum-free formulations with 1% BSA and 10 U/mL heparin, and the cells were starved for 4 h. DyLight 650-labeled FGF2 WT was added directly to the culture media in a concentration of 20 nM. The cells were preincubated with the protein for 40 min on ice, and then transferred to 37 °C for another 30 min. The cells were then detached from the culture plate with 5 mM EDTA-PBS and subjected for flow cytometric analysis using a NovoCyte 2060R instrument (ACEA Biosciences, San Diego, CA, USA) and NovoExpress software (version 1.6.1) (ACEA Biosciences).

### 3.11. Flow Cytometric Analysis of Conjugates' Steady-State Internalization

The method used for flow cytometric estimation of ligand internalization efficiency was adapted from the literature [62]. To determine the internalization yield, serum-starved HCC95, NCI-H520, NCI-H1581, JIMT-1, and G292 cells were treated with Alexa Fluor 555-labeled  $\alpha$ AMTN-FGF2<sub>V1</sub>, FGF2<sub>V2</sub>-MMAE, and  $\alpha$ AMTN-dFGF2<sub>V1V2</sub>-MMAE conjugates at a concentration of 2 nM, except for the group, where both  $\alpha$ AMTN-FGF2<sub>V1</sub> and FGF2<sub>V2</sub>-MMAE conjugates were added, at 1 nM concentration each. Incubation was carried out for 15 min at 37 °C. The cells were then rapidly placed on ice and extensively washed with ice-cold PBS in order to stop the receptor trafficking. Non-internalized conjugates were removed from the cell surface via multiple washes in acid stripping buffer (serum-free medium supplemented with 0.2% BSA, pH = 3.5). The cells were harvested with 5 mM EDTA-PBS and analyzed with a NovoCyte 2060R flow cytometer and NovoExpress software.

## 4. Conclusions

In summary, we developed a novel strategy for generating a dual-warhead cytotoxic conjugate through site-specific conjugation of cytotoxic payloads via SnoopLigase- and eSrtA-mediated ligation. Within this study, we explored  $\alpha$ AMTN, a selective and efficacious RNA polymerase II and III inhibitor derived from Amanita mushrooms, as well as a highly potent antimitotic agent, an analog of auristatin (MMAE), commonly used in antibody–drug conjugates (ADCs). Our results confirm that the FGF2 dimer with a specific well-defined topology can serve as an effective drug delivery vehicle for targeting cancer cells that overproduce FGFR1. Specifically, the  $\alpha$ AMTN-dFGF2<sub>V1V2</sub>-MMAE conjugate effectively kills cancer cells with high levels of FGFR1 while exhibiting minimal toxicity towards FGFR1-deficient cells. Our study successfully combines two distinct cytotoxic agents with the selective targeting properties of the FGF2 dimer, resulting in a highly potent and unique conjugate that has been validated in cellular models. The future research on the  $\alpha$ AMTN-dFGF2<sub>V1V2</sub>-MMAE dimeric dual-warhead conjugate should prioritize in vivo evaluation in murine models to comprehensively assess their therapeutic potential. These studies are necessary not only to confirm the anti-cancer efficacy of our molecule, but also to assess its systemic cytotoxicity. Importantly, we previously developed a monomeric FGF2-based conjugate that exhibited high toxicity against FGFR1-overproducing cancer cells in vitro and showed efficient tumor growth retardation in an FGFR-positive human breast cancer xenograft model in mice [63]. Administration of this FGF2-based conjugate did not cause any body weight loss or other side effects in the animals during the treatment period. These

data are very promising in the context of utilizing cytotoxic drug conjugates based on FGF2 in FGFR-targeted anti-cancer therapies.

**Supplementary Materials:** The following supporting information can be downloaded at: <https://www.mdpi.com/article/10.3390/ijms241210143/s1>.

**Author Contributions:** Conceptualization, D.N., M.A.K. and J.O.; methodology, D.N. and M.A.K.; validation, J.O.; investigation, D.N., M.A.K. and K.D.S.; resources, J.O.; data curation, D.N.; formal analysis, D.N.; writing—original draft preparation, D.N.; writing—review and editing, M.A.K. and J.O.; visualization, D.N.; project administration, J.O.; resources, J.O.; supervision, J.O.; funding acquisition, J.O. All authors have read and agreed to the published version of the manuscript.

**Funding:** The research leading to these results has received funding from the Norway Grants 2014–2021 via the National Centre for Research and Development, Project Contract No. NOR/POLNOR/DUALDRUG/0058/2019-00.

**Institutional Review Board Statement:** Not applicable.

**Informed Consent Statement:** Not applicable.

**Data Availability Statement:** Data will be made available on request.

**Acknowledgments:** We are extremely grateful to Malgorzata Zakrzewska for the insightful discussion and valuable feedback, which greatly helped us during the review process. We would like to acknowledge Marta Minkiewicz for her skillful assistance with cell culture maintenance.

**Conflicts of Interest:** The authors declare no conflict of interest.

## Abbreviations

|       |   |
|-------|---|
| ADC   | Antibody–drug conjugate.                            |
| ADCC  | Antibody-dependent cellular cytotoxicity.           |
| Ado   | 8-amino-3,6-dioxaoctanoyl.                          |
| ATCC  | American Type Culture Collection.                   |
| BSA   | Bovine serum albumin.                               |
| CDC   | Complement-dependent cytotoxicity.                  |
| DCM   | Dichloromethane.                                    |
| DIPEA | <i>N,N</i> -diisopropylethylamine.                  |
| DMAc  | <i>N,N</i> -dimethylacetamide.                      |
| DMF   | <i>N,N'</i> -dimethylformamide.                     |
| DTNB  | 5,5-dithio-bis-(2-nitrobenzoic acid).               |
| DTT   | Dithiothreitol.                                     |
| EC    | Effective concentration.                            |
| EDTA  | Ethylenediaminetetraacetic acid.                    |
| eSrtA | Evolved sortase A.                                  |
| FA    | Formic acid.  |
| FGF   | Fibroblast growth factor.                           |
| FGFR  | Fibroblast growth factor receptor.                  |
| HEPES | 4-(2-hydroxyethyl)-1-piperazineethanesulfonic acid. |
| HPLC  | High-performance liquid chromatography.             |
| HRP   | Horseradish peroxidase.                             |
| IPTG  | Isopropyl $\beta$ -D-1-thiogalactopyranoside.       |
| MALDI | Matrix-assisted laser desorption/ionization.        |
| MMAE  | Monomethyl auristatin E.                            |
| MS    | Mass spectrometry.                                  |
| TCEP  | Tris(2-carboxyethyl)phosphine.                      |
| OD    | Optical density.                                    |
| PABC  | Para-aminobenzylcarbamate.                          |
| PBS   | Phosphate-buffered saline.                          |
| PEG   | Poly(ethylene glycol).                              |
| PMSF  | Phenylmethylsulfonyl fluoride.                      |
| PVDF  | Polyvinylidene difluoride.                          |

|               |  |
|---------------|--|
| RP            | Reversed phase.  |
| SD            | Standard deviation.  |
| SDS-PAGE      | Sodium dodecyl sulfate polyacrylamide gel electrophoresis. |
| SPPS          | Solid phase peptide synthesis.                             |
| TB            | Terrific broth.  |
| TCA           | Trichloroacetic acid.                                      |
| TCE           | 2,2,2-trichloroethan-1-ol.                                 |
| TFA           | Trifluoroacetic acid.                                      |
| TIS           | Triisopropylsilane.  |
| TOF           | Time of flight.  |
| WT            | Wild-type.   |
| $\alpha$ AMTN | $\alpha$ -amanitin.  |

## References

1. Turner, N.; Grose, R. Fibroblast growth factor signalling: From development to cancer. *Nat. Rev. Cancer* **2010**, *10*, 116–129. [[CrossRef](#)]
2. Elsheikh, S.E.; Green, A.R.; Lambros, M.B.K.; Turner, N.C.; Grainge, M.J.; Powe, D.; Ellis, I.O.; Reis-Filho, J.S. FGFR1 amplification in breast carcinomas: A chromogenic in situ hybridisation analysis. *Breast Cancer Res.* **2007**, *9*, R23. [[CrossRef](#)] [[PubMed](#)]
3. Servetto, A.; Formisano, L.; Arteaga, C.L. FGFR signaling and endocrine resistance in breast cancer: Challenges for the clinical development of FGFR inhibitors. *Biochim. Biophys. Acta-Rev. Cancer* **2021**, *1876*, 188595. [[CrossRef](#)]
4. Katoh, M. FGFR inhibitors: Effects on cancer cells, tumor microenvironment and whole-body homeostasis (Review). *Int. J. Mol. Med.* **2016**, *38*, 3–15. [[CrossRef](#)]
5. Bange, J.; Pechtl, D.; Cheburkin, Y.; Specht, K.; Harbeck, N.; Schmitt, M.; Knyazeva, T.; Müller, S.; Gärtner, S.; Sures, I.; et al. Cancer progression and tumor cell motility are associated with the FGFR4 Arg388 allele. *Cancer Res.* **2002**, *62*, 840–847.
6. Kommalapati, A.; Tella, S.H.; Borad, M.; Javle, M.; Mahipal, A. Fgfr inhibitors in oncology: Insight on the management of toxicities in clinical practice. *Cancers* **2021**, *13*, 2968. [[CrossRef](#)] [[PubMed](#)]
7. Pacini, L.; Jenks, A.D.; Lima, N.C.; Huang, P.H. Targeting the fibroblast growth factor receptor (Fgfr) family in lung cancer. *Cells* **2021**, *10*, 1154. [[CrossRef](#)] [[PubMed](#)]
8. Javle, M.; Lowery, M.; Shroff, R.T.; Heinz Weiss, K.; Springfield, C.; Borad, M.J.; Ramanathan, R.K.; Goyal, L.; Sadeghi, S.; Macarulla, T.; et al. Phase II Study of BGJ398 in Patients With FGFR-Altered Advanced Cholangiocarcinoma. *J. Clin. Oncol.* **2018**, *36*, 276. [[CrossRef](#)] [[PubMed](#)]
9. Dai, S.; Zhou, Z.; Chen, Z.; Xu, G.; Chen, Y. Fibroblast growth factor receptors (Fgfrs): Structures and small molecule inhibitors. *Cells* **2019**, *8*, 614. [[CrossRef](#)]
10. Wu, C.P.; Hung, T.H.; Hsiao, S.H.; Huang, Y.H.; Hung, L.C.; Yu, Y.J.; Chang, Y.T.; Wang, S.P.; Wu, Y.S. Erdafitinib resensitizes ABCB1-overexpressing multidrug-resistant cancer cells to cytotoxic anticancer drugs. *Cancers* **2020**, *12*, 1366. [[CrossRef](#)]
11. Taberero, J.; Bahleda, R.; Dienstmann, R.; Infante, J.R.; Mita, A.; Italiano, A.; Calvo, E.; Moreno, V.; Adamo, B.; Gazzah, A.; et al. Phase I dose-escalation study of JNJ-42756493, an oral pan-fibroblast growth factor receptor inhibitor, in patients with advanced solid tumors. *J. Clin. Oncol.* **2015**, *33*, 3401–3408. [[CrossRef](#)]
12. Siefker-Radtke, A.O.; Mellado, B.; Decaestecker, K.; Burke, J.M.; O'Hagan, A.; Avadhani, A.N.; Zhong, B.; Santiago-Walker, A.E.; De Porre, P.; Brookman-May, S.; et al. A phase 2 study of JNJ-42756493, a pan-FGFR tyrosine kinase inhibitor, in patients (pts) with metastatic or unresectable urothelial cancer (UC) harboring FGFR gene alterations. *J. Clin. Oncol.* **2016**, *34*, TPS4575. [[CrossRef](#)]
13. Perera, T.P.S.; Jovcheva, E.; Mevellec, L.; Vialard, J.; De Lange, D.; Verhulst, T.; Paulussen, C.; Van De Ven, K.; King, P.; Freyne, E.; et al. Discovery & pharmacological characterization of JNJ-42756493 (Erdafitinib), a functionally selective small-molecule FGFR family inhibitor. *Mol. Cancer Ther.* **2017**, *16*, 1010–1020. [[CrossRef](#)]
14. Helsten, T.; Elkin, S.; Arthur, E.; Tomson, B.N.; Carter, J.; Kurzrock, R. The FGFR landscape in cancer: Analysis of 4,853 tumors by next-generation sequencing. *Clin. Cancer Res.* **2016**, *22*, 259–267. [[CrossRef](#)]
15. Javle, M.; Roychowdhury, S.; Kelley, R.K.; Sadeghi, S.; Macarulla, T.; Weiss, K.H.; Waldschmidt, D.T.; Goyal, L.; Borbath, I.; El-Khoueiry, A.; et al. Infigratinib (BGJ398) in previously treated patients with advanced or metastatic cholangiocarcinoma with FGFR2 fusions or rearrangements: Mature results from a multicentre, open-label, single-arm, phase 2 study. *Lancet Gastroenterol. Hepatol.* **2021**, *6*, 803–815. [[CrossRef](#)] [[PubMed](#)]
16. Xiang, H.; Chan, A.G.; Ahene, A.; Bellovin, D.I.; Deng, R.; Hsu, A.W.; Jeffrey, U.; Palencia, S.; Powers, J.; Zanghi, J.; et al. Preclinical characterization of bemarituzumab, an anti-FGFR2b antibody for the treatment of cancer. *MAbs* **2021**, *13*, 1981202. [[CrossRef](#)]
17. Catenacci, D.V.T.; Tesfaye, A.; Tejani, M.; Cheung, E.; Eisenberg, P.; Scott, A.J.; Eng, C.; Hnatyszyn, J.; Marina, N.; Powers, J.; et al. Bemarituzumab with modified FOLFOX6 for advanced FGFR2-positive gastroesophageal cancer: FIGHT Phase III study design. *Future Oncol.* **2019**, *15*, 2073–2082. [[CrossRef](#)] [[PubMed](#)]
18. Xiang, H.; Liu, L.; Gao, Y.; Ahene, A.; Collins, H. Covariate effects and population pharmacokinetic analysis of the anti-FGFR2b antibody bemarituzumab in patients from phase 1 to phase 2 trials. *Cancer Chemother. Pharmacol.* **2021**, *88*, 899–910. [[CrossRef](#)]

19. Wainberg, Z.A.; Enzinger, P.C.; Kang, Y.K.; Qin, S.; Yamaguchi, K.; Kim, I.H.; Saeed, A.; Oh, S.C.; Li, J.; Turk, H.M.; et al. Bemarituzumab in patients with FGFR2b-selected gastric or gastro-oesophageal junction adenocarcinoma (FIGHT): A randomised, double-blind, placebo-controlled, phase 2 study. *Lancet Oncol.* **2022**, *23*, 1430–1440. [[CrossRef](#)] [[PubMed](#)]
20. Meric-Bernstam, F.; Bahleda, R.; Hierro, C.; Sanson, M.; Bridgewater, J.; Arkenau, H.T.; Tran, B.; Kelley, R.K.; Park, J.O.; Javle, M.; et al. Futibatinib, an Irreversible FGFR1–4 Inhibitor, in Patients with Advanced Solid Tumors Harboring FGF/FGFR Aberrations: A Phase I Dose-Expansion Study. *Cancer Discov.* **2022**, *12*, 402–415. [[CrossRef](#)]
21. Bahleda, R.; Meric-Bernstam, F.; Goyal, L.; Tran, B.; He, Y.; Yamamiya, I.; Benhadji, K.A.; Matos, I.; Arkenau, H.T. Phase I, first-in-human study of futibatinib, a highly selective, irreversible FGFR1–4 inhibitor in patients with advanced solid tumors. *Ann. Oncol.* **2020**, *31*, 1405–1412. [[CrossRef](#)] [[PubMed](#)]
22. Sootome, H.; Fujita, H.; Ito, K.; Ochiwa, H.; Fujioka, Y.; Ito, K.; Miura, A.; Sagara, T.; Ito, S.; Ohsawa, H.; et al. Futibatinib is a novel irreversible FGFR 1-4 inhibitor that shows selective antitumor activity against FGFR-deregulated tumors. *Cancer Res.* **2020**, *80*, 4986–4997. [[CrossRef](#)] [[PubMed](#)]
23. Doi, T.; Shitara, K.; Kojima, T.; Kuboki, Y.; Matsubara, N.; Bando, H.; Yoh, K.; Naito, Y.; Hirai, H.; Kurokawa, Y.; et al. Phase I study of the irreversible fibroblast growth factor receptor 1–4 inhibitor futibatinib in Japanese patients with advanced solid tumors. *Cancer Sci.* **2023**, *114*, 574–585. [[CrossRef](#)] [[PubMed](#)]
24. Kim, S.M.; Kim, H.; Yun, M.R.; Kang, H.N.; Pyo, K.H.; Park, H.J.; Lee, J.M.; Choi, H.M.; Ellinghaus, P.; Ocker, M.; et al. Activation of the Met kinase confers acquired drug resistance in FGFR-targeted lung cancer therapy. *Oncogenesis* **2016**, *5*, e241. [[CrossRef](#)]
25. Yue, S.; Li, Y.; Chen, X.; Wang, J.; Li, M.; Chen, Y.; Wu, D. FGFR-TKI resistance in cancer: Current status and perspectives. *J. Hematol. Oncol.* **2021**, *14*, 23. [[CrossRef](#)]
26. Szlachcic, A.; Zakrzewska, M.; Loboeki, M.; Jakimowicz, P.; Otlewski, J. Design and characteristics of cytotoxic fibroblast growth factor 1 conjugate for fibroblast growth factor receptor-targeted cancer therapy. *Drug. Des. Devel. Ther.* **2016**, *10*, 2547–2560. [[CrossRef](#)]
27. Loboeki, M.; Zakrzewska, M.; Szlachcic, A.; Krzyscik, M.A.; Sokolowska-Wedzina, A.; Otlewski, J. High-Yield Site-Specific Conjugation of Fibroblast Growth Factor 1 with Monomethylauristatin E via Cysteine Flanked by Basic Residues. *Bioconjug. Chem.* **2017**, *28*, 1850–1858. [[CrossRef](#)]
28. Krzyscik, M.A.; Zakrzewska, M.; Sørensen, V.; Sokolowska-Wedzina, A.; Loboeki, M.; Swiderska, K.W.; Krowarsch, D.; Wiedlocha, A.; Otlewski, J. Cytotoxic Conjugates of Fibroblast Growth Factor 2 (FGF2) with Monomethyl Auristatin E for Effective Killing of Cells Expressing FGF Receptors. *ACS Omega* **2017**, *2*, 3792–3805. [[CrossRef](#)]
29. Swiderska, K.W.; Szlachcic, A.; Czyrek, A.; Zakrzewska, M.; Otlewski, J. Site-specific conjugation of fibroblast growth factor 2 (FGF2) based on incorporation of alkyne-reactive unnatural amino acid. *Bioorg. Med. Chem.* **2017**, *25*, 3685–3693. [[CrossRef](#)]
30. Świderska, K.W.; Szlachcic, A.; Opaliński, Ł.; Zakrzewska, M.; Otlewski, J. FGF2 dual warhead conjugate with monomethyl auristatin E and  $\alpha$ -amanitin displays a cytotoxic effect towards cancer cells overproducing FGF receptor 1. *Int. J. Mol. Sci.* **2018**, *19*, 2098. [[CrossRef](#)]
31. Krzyscik, M.A.; Opaliński, Ł.; Otlewski, J. Novel Method for Preparation of Site-Specific, Stoichiometric-Controlled Dual Warhead Conjugate of FGF2 via Dimerization Employing Sortase A-Mediated Ligation. *Mol. Pharm.* **2019**, *16*, 3588–3599. [[CrossRef](#)] [[PubMed](#)]
32. Nawrocka, D.; Krzyscik, M.A.; Opaliński, Ł.; Zakrzewska, M.; Otlewski, J. Stable fibroblast growth factor 2 dimers with high pro-survival and mitogenic potential. *Int. J. Mol. Sci.* **2020**, *21*, 4108. [[CrossRef](#)] [[PubMed](#)]
33. Ducry, L.; Stump, B. Antibody–Drug Conjugates: Linking Cytotoxic Payloads to Monoclonal Antibodies. *Bioconjug. Chem.* **2010**, *21*, 5–13. [[CrossRef](#)]
34. Reddy Chichili, V.P.; Kumar, V.; Sivaraman, J. Linkers in the structural biology of protein-protein interactions. *Protein Sci.* **2013**, *22*, 153–167. [[CrossRef](#)] [[PubMed](#)]
35. Chen, X.; Zaro, J.L.; Shen, W.C. Fusion protein linkers: Property, design and functionality. *Adv. Drug. Deliv. Rev.* **2013**, *65*, 1357–1369. [[CrossRef](#)]
36. Abdollahpour-Alitappeh, M.; Lotfinia, M.; Gharibi, T.; Mardaneh, J.; Farhadhosseinabadi, B.; Larki, P.; Faghfourian, B.; Sepehr, K.S.; Abbaszadeh-Goudarzi, K.; Abbaszadeh-Goudarzi, G.; et al. Antibody–drug conjugates (ADCs) for cancer therapy: Strategies, challenges, and successes. *J. Cell. Physiol.* **2019**, *234*, 5628–5642. [[CrossRef](#)]
37. Bushnell, D.A.; Cramer, P.; Kornberg, R.D. Structural basis of transcription:  $\alpha$ -amanitin-RNA polymerase II cocrystal at 2.8 Å resolution. *Proc. Natl. Acad. Sci. USA* **2002**, *99*, 1218–1222. [[CrossRef](#)]
38. Moldenhauer, G.; Salnikov, A.V.; Lüttgau, S.; Herr, I.; Anderl, J.; Faulstich, H. Therapeutic potential of amanitin-conjugated anti-epithelial cell adhesion molecule monoclonal antibody against pancreatic carcinoma. *J. Natl. Cancer Inst.* **2012**, *104*, 622–634. [[CrossRef](#)]
39. Chari, R.V.J.; Miller, M.L.; Widdison, W.C. Antibody-drug conjugates: An emerging concept in cancer therapy. *Angew. Chemie-Int. Ed.* **2014**, *53*, 3796–3827. [[CrossRef](#)]
40. Francisco, J.A.; Cervený, C.G.; Meyer, D.L.; Mixan, B.J.; Klussman, K.; Chace, D.F.; Rejniak, S.X.; Gordon, K.A.; DeBlanc, R.; Toki, B.E.; et al. cAC10-vcMMAE, an anti-CD30-monomethyl auristatin E conjugate with potent and selective antitumor activity. *Blood* **2003**, *102*, 1458–1465. [[CrossRef](#)]

41. Junutula, J.R.; Raab, H.; Clark, S.; Bhakta, S.; Leipold, D.D.; Weir, S.; Chen, Y.; Simpson, M.; Tsai, S.P.; Dennis, M.S.; et al. Site-specific conjugation of a cytotoxic drug to an antibody improves the therapeutic index. *Nat. Biotechnol.* **2008**, *26*, 925–932. [[CrossRef](#)]
42. Wang, L.; Amphlett, G.; Blättler, W.A.; Lambert, J.M.; Zhang, W. Structural characterization of the maytansinoid-monoclonal antibody immunoconjugate, huN901-DM1, by mass spectrometry. *Protein Sci.* **2005**, *14*, 2436–2446. [[CrossRef](#)] [[PubMed](#)]
43. Szakács, G.; Paterson, J.K.; Ludwig, J.A.; Booth-Genthe, C.; Gottesman, M.M. Targeting multidrug resistance in cancer. *Nat. Rev. Drug. Discov.* **2006**, *5*, 219–234. [[CrossRef](#)] [[PubMed](#)]
44. Baalman, M.; Ziegler, M.J.; Werther, P.; Wilhelm, J.; Wombacher, R. Enzymatic and site-specific ligation of minimal-size tetrazines and triazines to proteins for bioconjugation and live-cell imaging. *Bioconjug. Chem.* **2019**, *30*, 1405–1414. [[CrossRef](#)]
45. Liu, Y.; Tian, F.; Shi, S.; Deng, Y.; Zheng, P. Enzymatic Protein-Protein Conjugation through Internal Site Verified at the Single-Molecule Level. *J. Phys. Chem. Lett.* **2021**, *12*, 10914–10919. [[CrossRef](#)] [[PubMed](#)]
46. Buldun, C.M.; Jean, J.X.; Bedford, M.R.; Howarth, M. SnoopLigase Catalyzes Peptide–Peptide Locking and Enables Solid-Phase Conjugate Isolation. *J. Am. Chem. Soc.* **2018**, *140*, 3008–3018. [[CrossRef](#)]
47. Fierer, J.O.; Veggiani, G.; Howarth, M. SpyLigase peptide–peptide ligation polymerizes affibodies to enhance magnetic cancer cell capture. *Proc. Natl. Acad. Sci. USA* **2014**, *111*, E1176–E1181. [[CrossRef](#)]
48. Morgan, H.E.; Turnbull, W.B.; Webb, M.E. Challenges in the use of sortase and other peptide ligases for site-specific protein modification. *Chem. Soc. Rev.* **2022**, *51*, 4121–4145. [[CrossRef](#)]
49. Chuprakov, S.; Ogunkoya, A.O.; Barfield, R.M.; Bauzon, M.; Hickie, C.; Kim, Y.C.; Yeo, D.; Zhang, F.; Rabuka, D.; Drake, P.M. Tandem-Cleavage Linkers Improve the in Vivo Stability and Tolerability of Antibody-Drug Conjugates. *Bioconjug. Chem.* **2021**, *32*, 746–754. [[CrossRef](#)]
50. Chen, I.; Dorr, B.M.; Liu, D.R. A general strategy for the evolution of bond-forming enzymes using yeast display. *Proc. Natl. Acad. Sci. USA* **2011**, *108*, 11399–11404. [[CrossRef](#)]
51. Pishesha, N.; Ingram, J.R.; Ploegh, H.L. Sortase A: A Model for Transpeptidation and Its Biological Applications. *Annu. Rev. Cell. Dev. Biol.* **2018**, *34*, 163–188. [[CrossRef](#)]
52. Mao, H.; Hart, S.A.; Schink, A.; Pollok, B.A. Sortase-Mediated Protein Ligation: A New Method for Protein Engineering. *J. Am. Chem. Soc.* **2004**, *126*, 2670–2671. [[CrossRef](#)] [[PubMed](#)]
53. Schulz, E.; Karas, M.; Rosu, F.; Gabelica, V. Influence of the Matrix on Analyte Fragmentation in Atmospheric Pressure MALDI. *J. Am. Soc. Mass. Spectrom.* **2006**, *17*, 1005–1013. [[CrossRef](#)] [[PubMed](#)]
54. Wynes, M.W.; Hinz, T.K.; Gao, D.; Martini, M.; Marek, L.A.; Ware, K.E.; Edwards, M.G.; Böhm, D.; Perner, S.; Helfrich, B.A.; et al. FGFR1 mRNA and protein expression, not gene copy number, predict FGFR TKI sensitivity across all lung cancer histologies. *Clin. Cancer Res.* **2014**, *20*, 3299–3309. [[CrossRef](#)] [[PubMed](#)]
55. Jendryczko, K.; Rzeszotko, J.; Krzyscik, M.A.; Szymczyk, J.; Otlewski, J.; Szlachcic, A. Peptibody Based on FGFR1-Binding Peptides From the FGF4 Sequence as a Cancer-Targeting Agent. *Front. Pharmacol.* **2021**, *12*, 2811. [[CrossRef](#)]
56. Jendryczko, K.; Rzeszotko, J.; Krzyscik, M.A.; Kocyla, A.; Szymczyk, J.; Otlewski, J.; Szlachcic, A. Drug Conjugation via Maleimide-Thiol Chemistry Does Not Affect Targeting Properties of Cysteine-Containing Anti-FGFR1 Peptibodies. *Mol. Pharm.* **2022**, *19*, 1422–1433. [[CrossRef](#)]
57. Dutt, A.; Ramos, A.H.; Hammerman, P.S.; Mermel, C.; Cho, J.; Sharifnia, T.; Chande, A.; Tanaka, K.E.; Stransky, N.; Greulich, H.; et al. Inhibitor-sensitive fgfr1 amplification in human non-small cell lung cancer. *PLoS ONE* **2011**, *6*, e20351. [[CrossRef](#)]
58. Pahl, A.; Lutz, C.; Hechler, T. Amanitins and their development as a payload for antibody-drug conjugates. *Drug. Discov. Today Technol.* **2018**, *30*, 85–89. [[CrossRef](#)]
59. Lutz, C.; Simon, W.; Werner-Simon, S.; Pahl, A.; Müller, C. Total Synthesis of  $\alpha$ - and  $\beta$ -Amanitin. *Angew. Chemie-Int. Ed.* **2020**, *59*, 11390–11393. [[CrossRef](#)]
60. Chen, H.; Lin, Z.; Arnst, K.E.; Miller, D.D.; Li, W. Tubulin inhibitor-based antibody-drug conjugates for cancer therapy. *Molecules* **2017**, *22*, 1281. [[CrossRef](#)]
61. Mckertish, C.M.; Kayser, V. Advances and limitations of antibody drug conjugates for cancer. *Biomedicines* **2021**, *9*, 872. [[CrossRef](#)]
62. Li, N.; Hill, K.S.; Elferink, L.A. Analysis of Receptor Tyrosine Kinase Internalization Using Flow Cytometry. *Membr. Traffick.* **2008**, *21*, 305–317.
63. Krzyscik, M.A.; Zakrzewska, M.; Sørensen, V.; Øy, G.F.; Brunheim, S.; Haugsten, E.M.; Mælandsmo, G.M.; Wiedlocha, A.; Otlewski, J. Fibroblast Growth Factor 2 Conjugated with Monomethyl Auristatin e Inhibits Tumor Growth in a Mouse Model. *Biomacromolecules* **2021**, *22*, 4169–4180. [[CrossRef](#)]

**Disclaimer/Publisher’s Note:** The statements, opinions and data contained in all publications are solely those of the individual author(s) and contributor(s) and not of MDPI and/or the editor(s). MDPI and/or the editor(s) disclaim responsibility for any injury to people or property resulting from any ideas, methods, instructions or products referred to in the content.